Original Paper

Chao Kang · Su Chin Chen · Dave Chan · Samkele Tfwala

Numerical modeling of large-scale dam breach experiment

Abstract This paper presents the analysis of an earth dam breaching process which incorporates an analytical erosion model into CFX in ANSYS to calculate the rate of erosion in order to capture the kinematic characteristics of dam breach. Based on the water level and the storage capacity of the reservoir on the upstream side of the dam, the discharge of water over the dam can be calculated. The discharge of water is also used to validate the results from the numerical simulations. The height of the experimental dam during the breaching process is calculated using an empirical relationship based on the water level, the discharge rate, and the width of the breach. A particle-scale progressive scouring entrainment model has been incorporated into CFX in ANSYS to calculate the rate of erosion which is used to simulate the development of the breach. When comparing with field observations, the root-mean-square error (RMSE) between the calculated and measured surface velocities is equal to 0.37 m/s, indicating a discrepancy of 16%, and the RMSE of the calculated and measured discharge is equal to 1.13 m³/s, showing an average discrepancy of 19%. Additionally, the numerical results are validated by comparing the calculated and observed water levels in the breach and the calculated and observed width of the top of the breach. The RMSE between the calculated and observed water levels in the upstream of the dam (h_{up}), the water level in the center of the breach ($h_c + h_d$), and the width of the top of the breach (B_T) are equal to 0.026 m, 0.095 m, and 0.44 m, respectively, which show average discrepancies of 1%, 4%, and 13%, respectively. This dam break experiment is a unique full-scale experiment for the evaluation of numerical and analytical models. This research shows that the erosion model incorporated into CFX is able to capture the main characteristics of the dam failure process. The incorporation of the erosional model into the dam breach analysis can be used to analyze the failure process of barrier dams.

Keywords Dam breach · Progressive scouring model · Numerical modeling · Soil erosion · CFX

Introduction

Several dam failures occurring in the last couple of decades have resulted in catastrophic disasters (Singh Vijay and Scarlatos Panagiotis 1988). Examples are numerous, such as the failure of the Tous Dam in Spain (Alcrudo and Mulet 2007) and the Tangjiashan barrier dam in China (Chen et al. 2015b), which was the result of a massive debris flow of more than 20.4×10^6 m³ in volume and impounding of a lake with a volume of 315×10^6 m³ (Chen et al. 2011; Cui et al. 2012). In this event, a hydropower station upstream of the barrier dam was destroyed, and more than 70,000 people living downstream were affected. In addition, the Mount Polley tailings storage facility in Canada (Morgenstern et al. 2015) and the most recent (in 2018) Xe-Pian Xe-Namnoy Power Project dam in southern Lao (European Commission 2018) resulted in several villages being washed away with 35 casualties

and more than 6000 people displaced and hundreds reported missing.

Earth dams are generally composed of soil ranging from fine to coarse particles and built in a wide range of geomorphological setting, ranging from high debris avalanches to quick clay failures in wide valley floors (Fan et al. 2017). When an earth dam fails, the duration of the failure process may last from a few minutes to several hours or even several days (Alcrudo and Mulet 2007; Cui et al. 2012). Among various modes of failure of earth dams, overtopping is a common mode of failure (Gregoretti et al. 2010).

Large-scale dam breach experiments are difficult and costly to carry out. It requires an enormous volume of soil to construct the dam and a large quantity of water to simulate the breaching process. In addition, the breaching process must be carried out in a controlled manner with minimum impact on the environment while ensuring the safety of the people and surrounding infrastructures. It is for these reasons that most of the dam break experiments are conducted in a small-scale laboratory environment (Elkholy et al. 2016; Lauber and Hager 1998; Miller and Chaudhry 1989). Nonetheless, attempts have been made to conduct large-scale dam breach experiments. Kakinuma and Shimizu (2014) carried out a large-scale experiment in the Chiyoda experimental flume to study the mechanism of breaching the riverine levee. A two-dimensional numerical model, capable of capturing the widening process of the breach, has been proposed.

Elkholy et al. (2016) conducted dam breach flow experiments in the hydraulics laboratory at the University of South Carolina. The observed water level changes during the breach process agreed well with the analytical solution for the reservoir depth. Zhang et al. (2009) constructed a 9.7-m-high earth dam using cohesive, homogeneous soil. The conclusion emphasized that crest erosion is the major mechanism.

Macchione (2008) proposed a physically based dam breach numerical model to predict the peak discharge, outflow hydrograph, and different shapes of the dam. Two models were used to calculate the water level behind the dams with a triangular-shaped breach and a trapezoidal-shaped breach. The model gave good results in the simulation of several historical dam failures. In describing the breaching process, Biscarini et al. (2010) compared the three-dimensional Navier-Stokes model incorporating the volume of fluid discretization method with a simplified shallow water model using two-dimensional computational fluid dynamic (CFD). The results indicate that the three-dimensional model is able to describe the unsteady flow behavior in the whole process, while some discrepancies are observed between the experimental observations and numerical results from the two-dimensional shallow water model.

Yang et al. (2016) coupled the smoothed particle hydrodynamics (SPH) and element bending group (EBG) to model the interaction between the fluid and a flexible barrier in an open channel viscous flow with a free surface. Horizontal and vertical

displacements from experimental observations of the flexible barrier were compared with the numerical results. Haun et al. (2011) simulated flow over a trapezoidal broad-crested weir using Flow-3D and SSIIM2. The calculated discharge, flow height above the weir, and computation time were compared with the experimental results with an error of less than 2%.

Several formulations have been developed to calculate the rate of erosion of soil due to water flowing over a dam. Most of the equations are based on the phenomena of sediment transport on flow channel bed, which can be broadly classified as analytical models and empirical models. In the analytical models, there are basically two approaches to calculate the rate of erosion: the static approach and the dynamic approach. In static and dynamic approaches, force equilibrium and Newton's law of motion are applied on the erodible soil to calculate shear stresses and rate of erosion, respectively (Bouchut et al. 2016; Iverson and Ouyang 2015; Medina et al. 2008; Shrestha and Orlob 1996). In the empirical approach, the rate of erosion is related to the flow velocity and the net shear stresses by incorporating an empirical coefficient or other coefficients determined based on a large number of historical cases (Chen et al., 2015b; De Blasio et al. 2011; Lee and Mehta 1994). The diffusion process caused by the difference in sediment concentration between the erodible channel bed and the main body of the debris is also considered as one of the possible mechanisms of erosion (Egashira et al. 2001). It is noted that the current analytical approach in the calculation of the rate of erosion considers the shear failure of the soil in the channel bed. Static shear strength parameters are often used. Kang and Chan (2017) proposed an erosion model based on both sliding motion and rolling motion, and often, the rolling mechanism is an easier way for the soil to be eroded.

Although researchers have tried to study the development of dam breaching using different approaches, most of them focused on studying the dam failure process, calculating the change of water level after the failure and the widening process of the dam breach. There seem to no studies on the development process of the breach using a particle-scale erosional model, which describes the erosion characteristics better. The most practical approach is to study the process using a laboratory experiment to capture the real response of water and breach development. However, it is difficult to simulate field conditions in the laboratory with a limited number of tests and limited control of the required parameters to fully comprehend the hydraulic characteristics of the flow process. In addition, conducting experiments are time-consuming and expensive. Numerical simulations overcome some of these difficulties, and the test conditions can be easily varied to explore different flow characteristics. In addition, numerical simulations offer more detailed information of the flow process, such as shear stresses along the bottom of the breach, which vary during the development of the breach.

This paper presents the modeling of a dam breach by analyzing a unique full-scale field experiment conducted in Taiwan. The dam breach development process is explored based on field measurements. Flow characteristics and dam height are calculated based on equations developed for broad-weir dams. To model the breaching process, a particle-scale progressive scouring entrainment model has been incorporated into CFX in ANSYS to calculate the rate of erosion and to study the development of the breach. The erosion model was developed by Kang et al. (2017) and has

been validated through particle-scale numerical flume experiment (Kang and Chan 2018a) and the study of historical cases (Kang et al. 2017; Kang and Chan 2018b). However, this model has not been used to calculate the rate of erosion resulting from water flow in a dam breach. Compared to a previous study in which the shear stress was calculated based on a simple sliding model, the shear stress in this simulation is calculated based on 3D topography of the channel in CFX and incorporating the viscosity of water, which is not usually considered in traditional erosional models. The calculated eroded depth is used to adjust the height of the erodible bottom of the breach at a specified time. The simulation results are verified by comparing the discharge rate, flow height, and the width at the top of the breach with field observations.

Dam breach experiment

Description of the experiment

A large-scale dam breach experiment was conducted at Landao Creek in Huisun Forest, National Chung Hsing University, Taiwan, on May 22, 2015 (Fig. 1a). Huisun Forest is located at an elevation of 450 m at the Greeting Green Bridge to 2419 m on the Shou-Cheng Grant Mountain. These changes in elevations in the geographical environment provide subtropical, warm belts and temperate climates, as evidenced by the vegetation in this area.

A reservoir is located above the mountain, which has a discharge channel with a manual control gate that can release water down the channel. The channel is approximately 25 m in width and 3 m in height, respectively. Material lying on the flow channel bed mainly consisted of loose granular particles and was used to construct the earth dam. The channel in the study area was 700 m, with a slope of approximately 6.3°. Figure 1 b shows the experimental dam, which had a cross section of a trapezoid shape. The width at the crest was 2 m, and the upstream and downstream slopes of the dam were around 30° with respect to the horizontal. The height of the dam was 2.806 m, with a length of 24 m (Fig. 1b).

Nengkau irrigation system from a sluice gate provided the water for the experiment at the upstream of Landao Creek. During the test, two water level loggers were placed at the upstream side of the dam to monitor the variation of water levels by measuring the water pressure. Photogrammetry was used to determine the development of the breach based on a grid painted on the downstream face. Surface velocities of water flow were measured at specified times using foam buoys dropping from the upstream of the dam. Three-dimensional light detection and ranging (LiDAR) was used to accurately measure the channel elevations before and after the experiment.

According to the water level measurements, both using piezometers and the relationship between water level and the volume of water on the upstream side of the dam, it is possible to calculate the steady-state flow rate of the creek, which is estimated to be approximately 0.5 m³/s. Water reached the dam at around 11:25 am on May 22, 2015, and breaching of the dam was observed around 11:44 am.

Elevations of the flow channel

Based on the measurements from LiDAR, the relative coordinates of the points on the channel surface can be obtained, and a digital
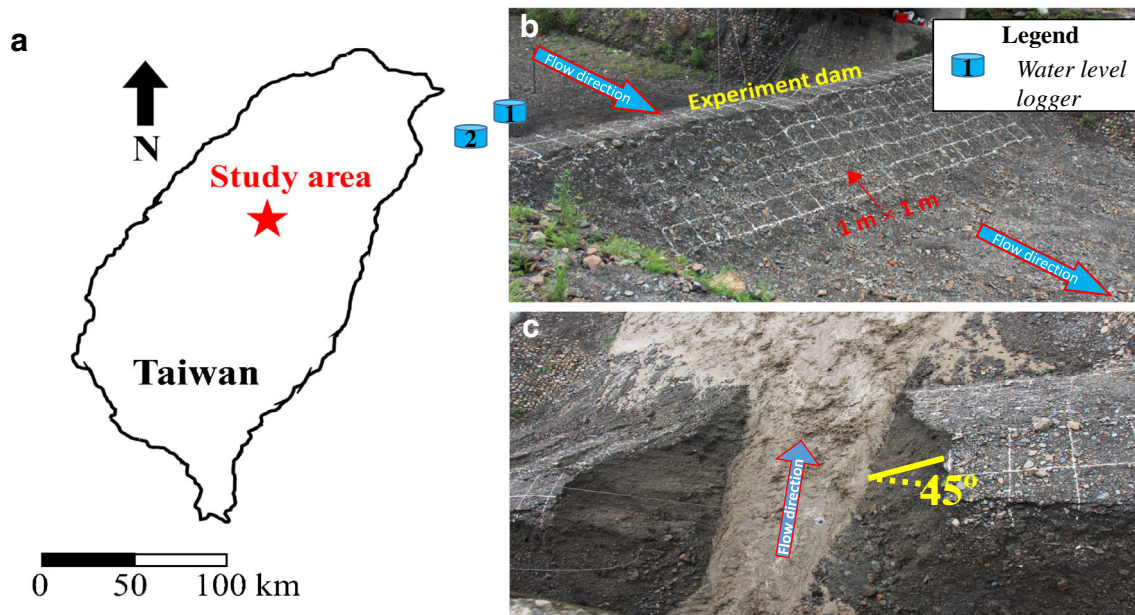
Fig. 1 Information of the study area. **a** Location of the study area. **b** Photo of dam taken from the right side downstream. **c** Photo of dam after failure which was taken from the top of the dam

elevation model (DEM) with a resolution of 0.1 m × 0.1 m is created based on the obtained x, y, and z coordinates (Fig. 2). The change of elevation in the three-dimensional map is differentiated by different colors assigned for each elevation. Figure 2 a and b show the terrain before and after the event. The dam is labeled in the diagram. Samples were obtained for grain size analysis, and the locations of the sampling points are denoted as C and D, representing the locations in the channel and on the dam, respectively, as shown in Fig. 2. To understand the changes in elevations before and after the event, the elevation of the terrain after the event is subtracted from that before the event as shown in Fig. 2 c. The analysis of dam erosion here is focused on the dam breach event from the start of the breaching of the dam to the point when the water on the upstream side was almost fully discharged. This process took about 2 to 3 min.

The longitudinal profile along the channel is shown in Fig. 3 a. During the dam breach event, both erosion and deposition were observed along the channel (Fig. 3b). The average deposition height along the channel downstream of the dam is approximately 0.30 m. During the release of water from the reservoir upstream, a considerable amount of material had been transported from the channel bed upstream and deposited on the upstream side before the dam breach. This is indicated by an increase in the elevation of channel bed on the upstream side after the event (Fig. 3b). The eroded material from the dam was deposited in the downstream of the dam.

Figure 1 c provides the top view of the dam during the development of the dam breach. The angle of slopes of the side banks of the breach is about 45°, based on the digital elevation model after the event. Since the banks of the breach were formed during a natural erosional process, the angle of the banks should be close to the angle of repose of the material, which is about 45° as well.

Variation of water level

Figure 4 a shows the variation of water levels starting from a few minutes before the water reaches the dam. The water level is calculated based on piezometers located close to the toe of the dam at the upstream side. The water level on the upstream side started to rise at 11:30 am and reached its peak at 11:44 am. However, the water level decreased from the peak value to a relatively constant level in 3–4 min.

Figure 4 b shows the relationship between the water levels and the volume of water on the upstream side, which is calculated according to DEM before the failure of the dam. The storage capacity of the dam is equal to 1005 m³. This is the *static* storage capacities of the reservoir. During dam failure, there was a continuous inflow of approximately 0.5 m³/s from upstream of the dam. Therefore, the actual volume of water flowing through the dam breach is larger than the water storage before the dam breach.

The particle-size distribution of the channel before and after the event

Specimens were sampled at three locations in the channel before and after the experiment (Fig. 2). Together with the specimen sampled from the dam, a total of five specimens were used in the sieve analysis. Figure 5 shows the particle-size distribution of all the samples. Overall, the size of the particles in the dam is finer than that lying on the channel bed. After the experiment, finer particles were eroded by the water. Meanwhile, coarser particles were left behind in the flow channel.

Breaching process in the field experiment

The breaching process in the experiment is generally classified into two stages: the initial breaching stage and the breach development stage (Yang et al., 2016; Zhang et al. 2019). In this experiment, a 3-m wide breach has been formed manually before the experiment. Therefore, the experiment started from the breach development stage.
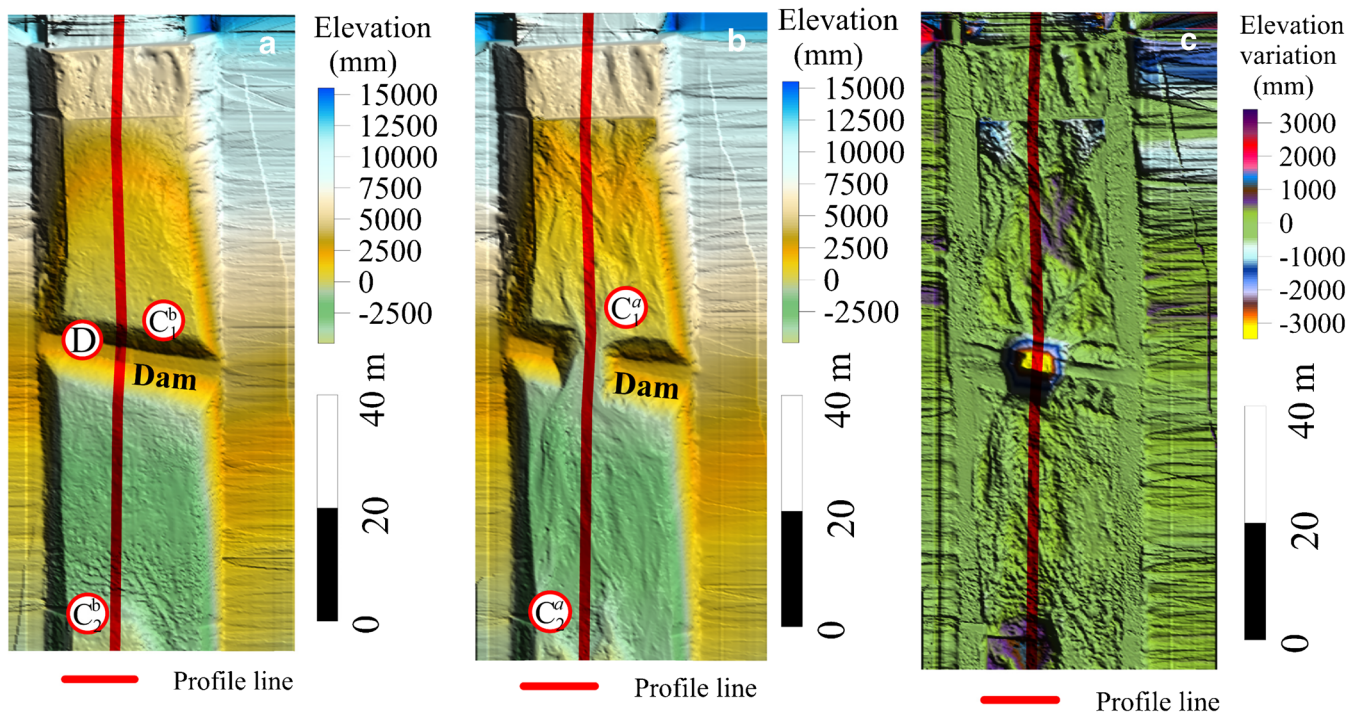
Fig. 2 Elevations of the flow channel before and after the experiment. **a** Before dam failure. **b** After dam failure. **c** Differences in elevations. C and D are the locations of the sample points. The subscript denotes the sample number. The superscripts a and b denote after and before the experiment, respectively

Once the overtopping was detected, the dam material started to be eroded, which mainly occurred in the developed beach. Erosion of the banks on either side of the breach was not very obvious. However, this stage only lasted for a few seconds, and the surface velocity of water was small. After a few more seconds, the water discharge was visibly increased, and the boundaries of the breach started to extend laterally. Meanwhile, the

increase in discharge and the lowering of water surface indicated that erosion occurred at the bottom of the breach. The discharge continued to increase, resulting in the enlarging of the breach. In this process, the banks of the breach developed into an almost constant slope angle accompanied by erosion at the bottom of breach. Since the dam was constructed using loose granular material, the slopes of the banks were close to
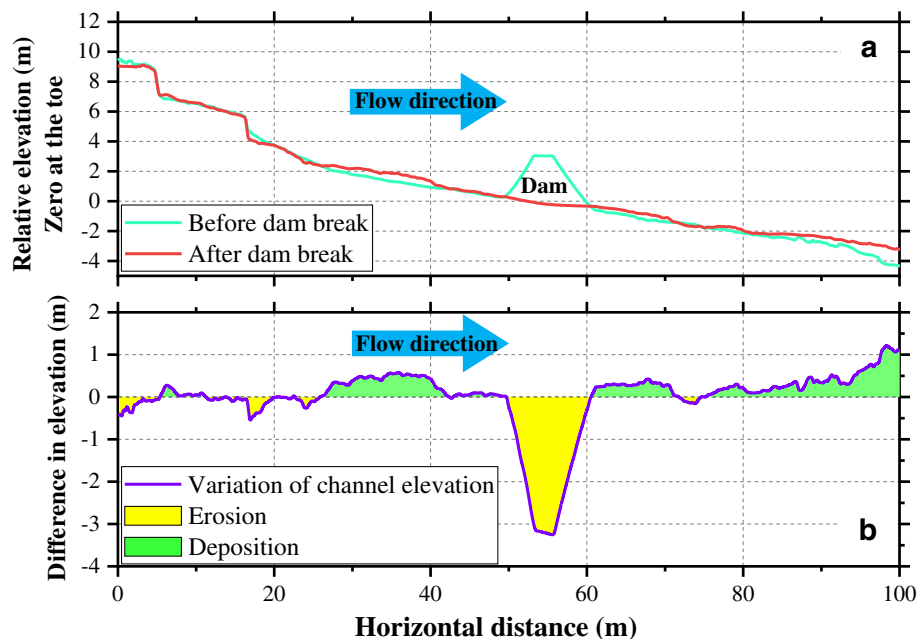

Fig. 3 The elevation and its change along the longitudinal profile. **a** The relative elevation of channel bed before and after the dam breach. **b** Difference in elevation along the profile line
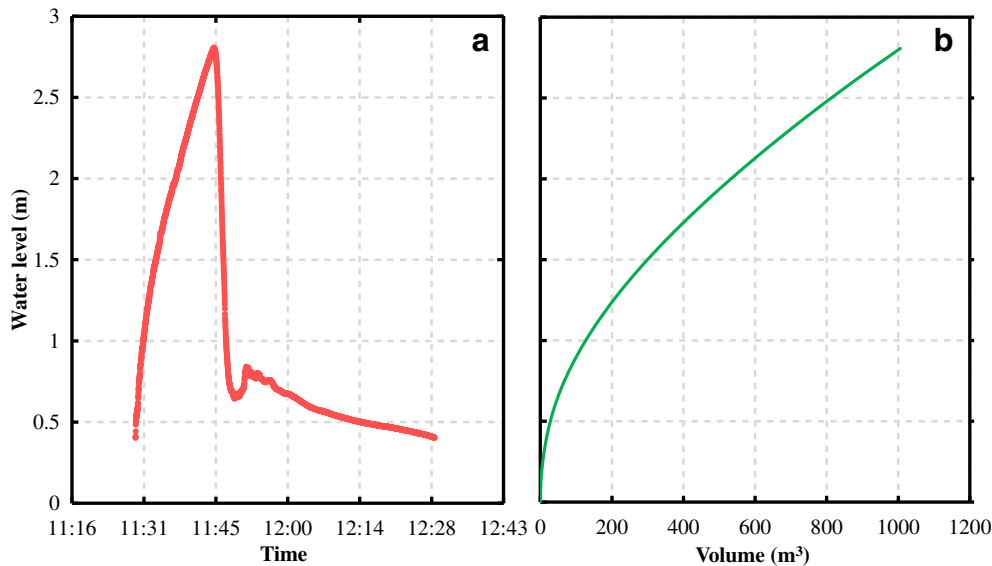
Fig. 4 **a** Variation of water levels at the upper stream of the dam. **b** Relationships between water level and water volume behind the dam

the angle of repose of the material, which was approximately equal to 45°. After around 160 s, the water surface behind the dam was close to the water surface height in the breach. The boundaries of the banks of the breach almost stopped extending, and the discharge of water behind the dam became constant, which was approximately equal to the inflow rate, indicating the end of the main breaching process.

Calculating the dam breach

In most dam breach models, the discharge through the breach is estimated using an equation for a broad-crested weir (Chen et al., 2015b). Shi et al. (2015) studied the erosion process of a breach due to water flow in the Tangjiashan barrier dam and considered that the cross section of the breach developed downward is a trapezoid shape. The erosion process was divided into three stages. In the

first stage, the main erosion characteristic was the change of the slope of the banks in the breach, which finally reached the angle of repose of the dam material. In the second stage, the erosion occurred on the banks and the bottom of the breach. The last stage consisted of mainly the erosion of the banks of the breach. Ng et al. (2013) also recognized that the trapezoidal shape of a channel could model the channelized topography. Ahmad and Azamathulla (2012) derived an equation to calculate the discharge over a weir with a trapezoidal breach.

According to the assumption of the occurrence of parallel critical flow on the crest, Azimi et al. (2013) derived the discharge equation for flow over a finite crest length weir as follows:

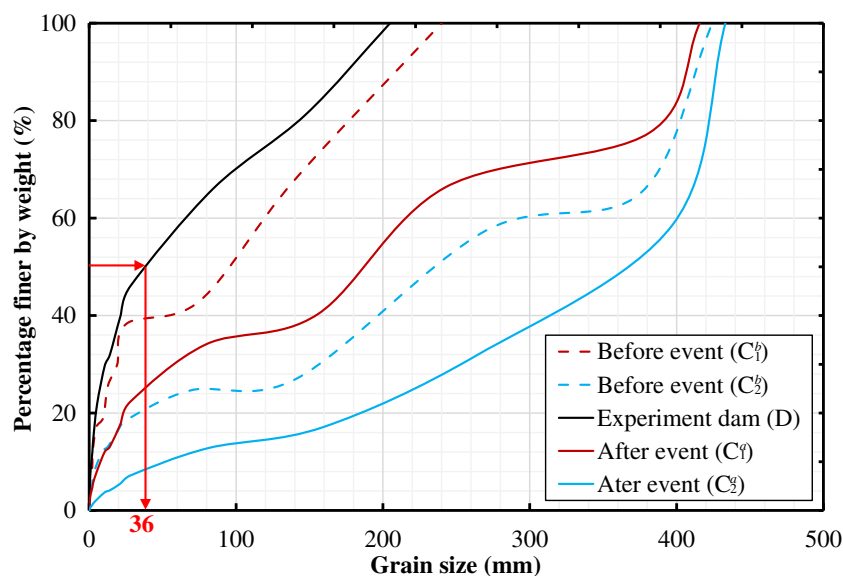$$Q = C_d B \sqrt{8/27} \sqrt{g} h^{3/2} \tag{1}$$

Fig. 5 Particle-size distribution curve of soil samples along the flow path. The meanings of superscript and subscript refer to the caption of Fig. 2

where Q is the rate of discharge, C_d is the discharge coefficient, B is the width of the channel in which the weir is installed perpendicularly to the flow direction, h is the head over the weir, and g is the gravitational acceleration.

Azimi et al. (2013) developed the correlations between discharge coefficient (C_d) and water head (h) over a weir, and length of the crest (L), for different shapes of weirs, including rectangular, trapezoidal (embankment), and triangular (hump) weirs. In the field experiment, a trapezoidal-shaped weir was constructed. The equation for the calculation of C_d for a trapezoidal weir proposed by Azimi et al. (2013) can be determined from

$$C_d(L_w/L)^{-1/10} = 0.688\left(\frac{h}{h+L_w}\right)^2 + 0.405\left(\frac{h}{h+L_w}\right) + 1 \qquad (2)$$

where L_w is the width of the bottom of a breach in the flow direction, which is a function of h_d and slope angle of the dam (β). The slope angle of the dam surface can be calculated from the dam profile. For the experimental dams in Taiwan, the slope angle is around 30°. L is the width of the dam at the base as indicated in Fig. 6 a.

According to Fig. 6, the height of water in the breach (h) is equal to $h = h_f - h_d$, in which h_f is the flow height and h_d is the dam height. To find the relationship between B, the width of the water surface in the breach, and h_c and h, it is assumed that the ratio of the average width of the breach to the height of the trapezoid shape is constant. The average width of the breach is the average value of the top and bottom widths. This idea is based on a modification of the erosion model from Shi et al. (2015) and Chang and Zhang (2010). Chang and Zhang (2010) assumed that the rates of erosion of the bottom and the banks of the breach are the same. This assumption is not applicable in this case since the erosion mechanism is quite different for the banks and the bottom of the breach.

In this paper, since the dam material is basically homogeneous, the slope of the two sides of the breach is assumed to be a constant during the flow process. The slope angle of the two sides of the trapezoid is measured from the digital elevation model after the dam failure, which is equal to 45° for this case. Therefore, a relationship can be derived as follows:

$$\frac{B + H - 2h_c - h_d}{H - h} = C \qquad (3)$$

where H is the total height of the dam before the development of the breach, which is equal to 2.806 m. The constant C, calculated according to the final shape of the dam, is equal to 3.01 in this experiment. The height of the water over the breach (h_c) can be related to ($h_f - h_d$) based on continuity and Bernoulli's equations at the critical flow condition, for $Fr = 1$, based on rectangular flow channel.

In summary, in Eqs. (1), (2), and (3), the unknowns are Q, h_f, and h_d. From field measurements of water level and the relationship between water surface and storage volume on the upstream side, Q and h_f can be determined. Using MATLAB, a numerical solution of h_d is obtained.

The dam heights are calculated according to the heights of the water flow and the discharge rates from the breach after dam failure. Figure 7 shows the calculated dam height at the beginning of breaching to about 250 s based on Eqs. (1) to (3). In the initial 130 s, the dam height decreases continuously. However, after that, the calculated dam height is around 0.5 m, with variations of 0.2 m. The measured water level in the field varied after around 130 s, which may be caused by the failure of the banks in the breach, which resulted in an increase of the elevation of the bottom of the breach. Therefore, this explains the variations in the calculated dam height. After failure, the height of the base of the breach above the toe of the dam (h_d) is equal to 0.65 m.

Numerical simulation of dam breach

The dam breach in the experiment is a three-dimensional process. Therefore, a three-dimensional numerical model with the capability to remove part of the dam to simulate the breaching process is required. The element-based finite volume method CFX 15.0 in ANSYS is used in the simulation. The breaching process is simulated by removing layers of elements in the CFX model, and the height of each layer is determined by the progressive scouring entrainment model proposed by Kang and Chan (2017).

The rate of erosion is determined according to the drag force calculated at the interface between water and the dam using the velocities obtained from CFX. Based on the rate of erosion at a specific time in the modeling process, the thickness of the layer of material which will be eroded can be calculated. The CFX finite element model is then re-meshed to remove the elements in the eroded layer. The elapsed time to remove the first layer is determined based on field observation, according to Fig. 7. The process is repeated from the beginning to the end of the dam breach process.

Governing equations in CFX

In CFX, the governing equations are three-dimensional Reynolds-averaged Navier-Stokes equations and continuity equation. In the Navier-Stokes equations, the k-ε model is used to calculate the increase of viscosity due to turbulence. The governing equations are

$$\frac{\partial \rho u_i}{\partial x_i} = 0 \qquad (4)$$

$$\frac{\partial \rho u_i}{\partial t} + \frac{\partial \rho u_i u_j}{\partial x_j} = -\frac{\partial p}{\partial x_i} + \frac{\partial}{\partial x_i}\left[(\mu + \mu_t)\left(\frac{\partial u_i}{\partial x_j} + \frac{\partial u_j}{\partial x_i}\right) - \frac{2}{3}\rho k \delta_{ij}\right] \qquad (5)$$

where x_i is the distance in the i direction, u_i is the velocity in the i direction, t is the time, ρ is the density, k is the turbulent kinetic energy, δ_{ij} is the Kronecker delta, p is the pressure, μ is the viscosity, μ_t is the viscosity due to turbulence, and g_i is the force of gravity in the i direction. This is a system of equations in which subscript i refers to the x, y, or z directions in Cartesian coordinates. The turbulent viscosity is calculated from $\mu_t = \rho C_\mu k^2/\varepsilon$, where ε is the dissipation rate. The values of k and ε are
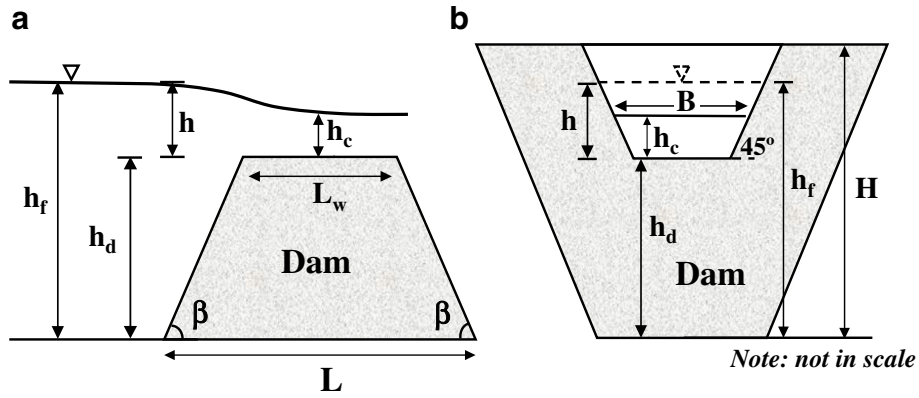
Fig. 6 Definition of each symbol in the calculation (not in scale). **a** Longitudinal profile along the flow channel. **b** Cross section along the dam

determined based on the differential transport equations for the turbulence kinetic energy and turbulence dissipation rate

$$\frac{\partial \rho k}{\partial t} + \frac{\partial \rho k u_j}{\partial x_j} = \frac{\partial}{\partial x_j}\left[\left(\mu + \frac{\mu_t}{\sigma_k}\right)\frac{\partial k}{\partial x_j}\right]$$
$$+ \mu_t\left(\frac{\partial u_i}{\partial x_j} + \frac{\partial u_j}{\partial x_i}\right)\frac{\partial u_i}{\partial x_j} - \rho\varepsilon \quad (6)$$

$$\frac{\partial \rho\varepsilon}{\partial t} + \frac{\partial \rho\varepsilon u_j}{\partial x_j} = \frac{\partial}{\partial x_j}\left[\left(\mu + \frac{\mu_t}{\sigma_\varepsilon}\right)\frac{\partial \varepsilon}{\partial x_j}\right] + C_1\frac{\varepsilon}{k}P_k - C_2\rho\frac{\varepsilon^2}{k} \quad (7)$$

where C_μ, C_1, C_2, σ_k, and σ_ε are constants. In the calculation, the default values of these parameters for the water are $\rho = 997$ kg/m^3, $\mu = 0.001$ Pa/s, $C_1 = 1.44$, $C_2 = 1.92$, $\sigma_k = 1.0$, $\sigma_\varepsilon = 1$, and $C_\mu = 0.09$, which are adopted in the CFX model (CFX 2009; Langford et al. 2016).

In multiphase flow modeling, the volume of fluid (VOF) method is used. This method introduces an additional variable β to consider the volume fraction for gas and liquid phase in each control volume. The time-averaged governing equation is given by

$$\frac{\partial \rho\varepsilon}{\partial t}\frac{\partial \beta}{\partial t} + \overline{u}_i\frac{\partial \beta}{\partial x_i} = 0 \quad (8)$$

For two-phase flow, $\beta = 1$ represents that the control volume is completely filled with one of the phases, while $\beta = 0$ means it is completely filled with the other phase.

The domain of the numerical model extends up to approximately 50 m upstream of the dam. An unstructured tetrahedral mesh is used in the numerical simulations, with a local spherical refinement area close to the breach. For the entire domain, the maximum element size is 0.25 m, with inflation layers (0.01 m) at the interfaces between water and boundaries. The finer mesh in the spherical area (6 m in diameter) includes the whole breach body with element sizes of 0.05 to 0.1 m. The inflation zone starts with 0.01 m, and the size is increased at a ratio of 1.2.
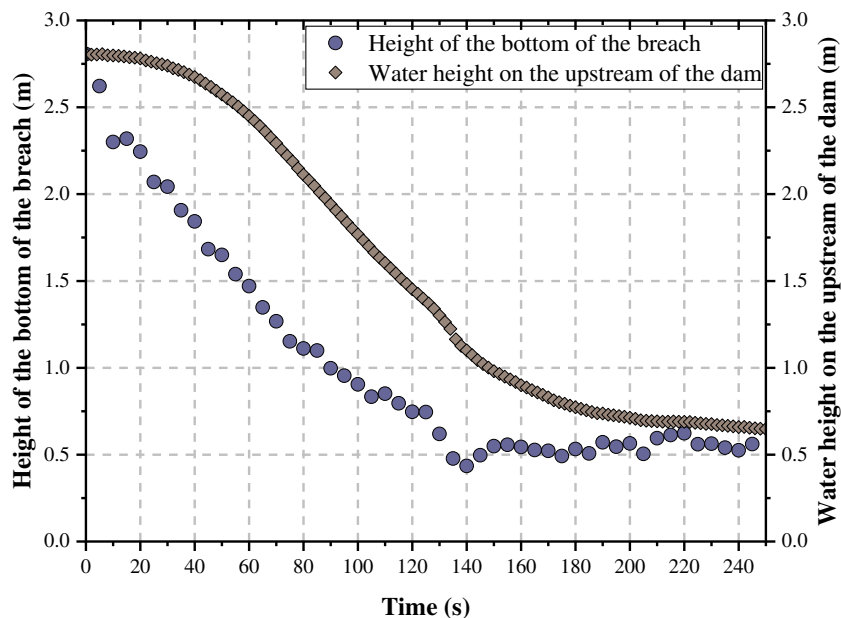

Fig. 7 Calculated height of the bottom of the breach based on the observed water height on the upstream of the dam

The velocities (u_1, u_2, and u_3) of the water in the reservoir are set to zero at the beginning of the simulation, and the water pressure is considered to be hydrostatic based on the water depth in the computation zone. The top velocity and gradient of the computation opening are zero. Each layer surface is set as no slip wall. The roughness of the layer surface is calculated based on the characteristic particle size used in the erosion model and particle arrangement. An inflow of 0.5 m³/s is also included in the simulation to consider recharge from the creek, which is calculated based on the water level variation before the development of dam breach. The water level in the reservoir behind the dam is equal to the dam height at the beginning of the simulation. The total volume of the reservoir on the up-stream side is equal to 1005 m³. The dam length in the transverse direction and the initial dam height are 24 m and 2.806 m, respectively. The length of the water surface in the longitudinal direction is 25 m.

Velocity and drag forces at the base of the breach

When water flows over the base of the breach, it applies a drag force on the bottom of the breach, which causes erosion of the soil particles lying on the bed. The drag force applied on the particles consists of two components: drag forces due to pressure gradient and surface friction due to shear stresses. The drag force can be approximatively calculated using the equation $T = C_D A \rho U^2 / 2$, in which T is the total drag force, C_D is the drag coefficient, and A is the projected area of the protruded part of a particle above the plane perpendicular to the flow direction. Theoretically, the velocity (U) is the relative velocity along the flow direction close to the channel surface. However, the relative velocity is very difficult to obtain in practice. Therefore, the maximum velocity, which is the surface velocity here, is used instead (Kelbaliyev, 2011). The difference between the relative velocity and surface velocity has been considered in the selection of the drag coefficient. In the calculation, the drag coefficient ranges from 0.7 to 0.8 for different α_o values, according to Blevins (1984). The projected area (A) is a function of the particle size and the value of α_o. Flow velocities are calculated in CFX in the middle of the dam at different stages of breaching. The calculated total drag force is shown in the section "Rate of erosion."

Figure 8 shows the horizontal velocities of water at different depths. The horizontal velocities are almost constant with depth except at the interface between water and dam. As shown in Fig. 8, the maximum velocity is around 3.32 m/s at 70 s.

Shear stresses which resulted from surface friction can be calculated at the same location. Shear stresses are calculated based on the relationship between shear velocity and bed shear stress in the CFX. The shear velocity is calculated using a logarithmic law of wall iterative procedure (CFX 2009), in which a velocity at a certain distance from the boundary, modulus of elasticity for water, and kinematic viscosity of water are used. In the calculation, non-zero shear stress is only observed close to the interface of the base and water as shown in Fig. 9. This is due to the rapid change in velocities close to the water and soil interface, and the velocity profiles are relatively constant in the water. Through the comparison of the total drag force and the shear force due to shear stress, it is noted that approximately no more than 10% of the drag force comes from the shear component.

Calculating the rate of erosion

Model description

In general, a spherical particle can be moved by both rolling and sliding motions. However, most of the time, only the sliding motion is considered in the erosion model. According to the analysis of the required force for both rolling and sliding motions, the drag force to initiate the rolling motion is less than that required for sliding motion (Wu and Chou 2003; Cheng et al. 2003; Shodja and Nezami 2003). Therefore, Kang and Chan (2017) developed a 2D particle-scale progressive scouring entrainment model to capture both rolling and sliding motions, which is used to calculate the rate of erosion caused by the breaching of the dam. The model is mainly focused on the calculation of the rate of erosion downward.

In the derivation of the equation used to calculate the rate of erosion, a spherical particle is assumed with a characteristic particle size of R. Once the drag force overcomes the required force for rolling motion, which is less than that for sliding motion (Kang and Chan 2017), the particle will roll around the contact point O (O_t means point O at time t) with the adjacent particle located downstream (Fig. 10). The rolling motion is governed by Newton's law of motion, which is given by

$$\frac{TR}{(I + mR^2)}\sin\alpha_t - \frac{mgR}{(I + mR^2)}\cos(\alpha_t + \theta) = \frac{\partial^2\alpha_t}{\partial t^2} \tag{9}$$

where T is the drag force applied on the center of the particle, I is the moment of inertia when particle rotates along the axis across the center of a particle (cylinder for 2D), m is the mass of the particle, ρ_b is the density of the particle, α_t is the angle between the channel bed and connection line of the centers of those two particles, θ is the slope angle of the channel bed, g is the gravity acceleration, $\partial^2\alpha_t / \partial t^2$ is angular acceleration, and t is time (Kang and Chan 2017).

For sliding motion, the translational acceleration ($\bar{a}$) is calculated from

$$\overline{a} = \frac{1}{m\cos\alpha_t}\left(N\sin\alpha_t - mg\cos\theta - F^{'}\cos\alpha_t\right) \tag{10}$$

where N is the reaction force and F' is the frictional force between two adjacent particles with opposing frictional forces (F) (Kang and Chan 2017). If rolling and sliding motions occur during an erosion process, Eqs. (9) and (10) should be used to calculate the accelerations.

Once the time required for a particle to rotate or slide over an adjacent particle located downstream (t_i) is calculated according to Eqs. (9) and (10), the rate of erosion per unit area for a given α_o can be obtained from

$$\ddot{E}_i = \frac{2R\sin\alpha_{oi}}{t_i} \tag{11}$$

To eliminate the discontinuity of the particle-scale progressive scouring erosion model, the possible locations of two adjacent particles are considered by introducing a probability density
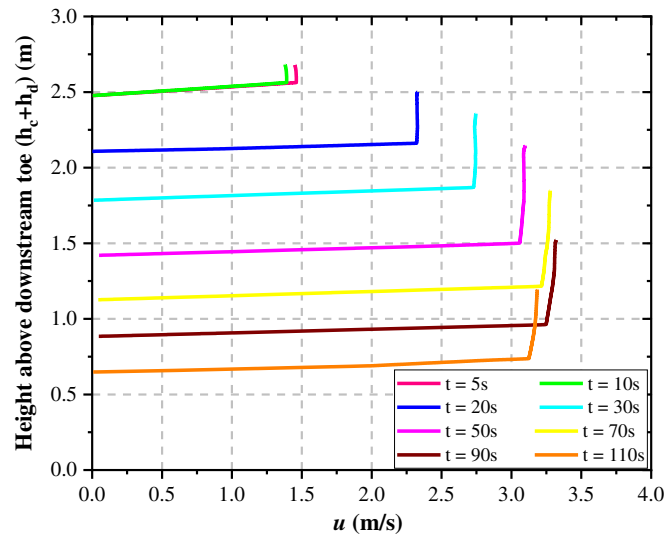
Fig. 8 Horizontal velocities of water at different depths and time at the center of the dam

function (PDF), which is used to describe the spatial variation of α_o. Therefore, the rate of erosion ($\dot{E}$) can be determined from the rate of erosion of an individual particle ($\dot{E}_i$) and the probability (P_i) of a certain value of α_o

$$\ddot{E} = \sum_{i=1}^{n} \left(\ddot{E}_i P_i \right) \qquad (12)$$

where n is the number of divisions of the probability density function in the approximation over the range of the values of α_o. For more details of the progressive scouring erosion model, refer to Kang and Chan (2017).

Selection of parameters

In the progressive scouring model, the parameters mainly include the density of the particles, drag force existing on the erodible bed, mean value of α_o in PDF, and the characteristic size of particles. In modeling the dam breach experiment, since the granular particles are eroded by water, it is considered that particles are fully saturated without excess pore water pressure. Therefore, only the buoyancy force is incorporated by subtracting the density of water from the density of particles. The drag force is calculated based on velocities in the simulation using CFX in a 10-s interval. In each time interval, the drag force is considered to be constant. Since the variation of the drag force is not large from time to time due to the relatively steady flow of water over the breach, this approximation would not lead to a significant error in the results.

Theoretically, for the same size particle lying on a slope with a constant angle, the rate of erosion is approximately directly proportional to the drag force when the drag force applied overcomes the resistance of rolling motion. In this dam breach case, since the dam was constructed using a mixture of granular material, it is
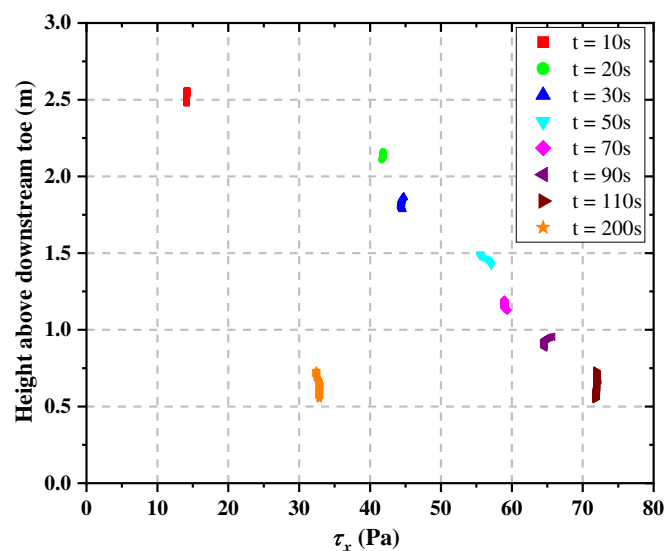

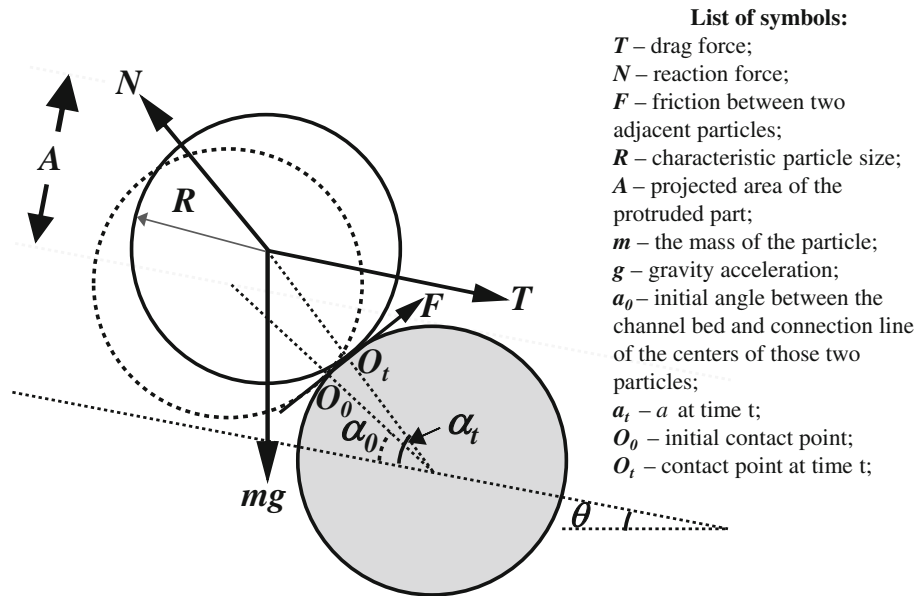**Fig. 9** Distribution of shear stress along the flow depth at the different times

Fig. 10 Illustration of forces acting on an eroding particle

List of symbols:
T – drag force;
N – reaction force;
F – friction between two adjacent particles;
R – characteristic particle size;
A – projected area of the protruded part;
m – the mass of the particle;
g – gravity acceleration;
a_0 – initial angle between the channel bed and connection line of the centers of those two particles;
a_t – a at time t;
O_0 – initial contact point;
O_t – contact point at time t;

considered that the particle-size distribution of granular material in each layer is similar. Characteristic particle size is used to represent the particle-size distribution of the material in the dam. The selection of this parameter is based on analysis of granular material carried out by Kang et al. (2017) and Kang and Chan (2018a).

Chang and Zhang (2010) studied the dam failure process, keeping the base of the breach horizontal. In this study, the bottom of the breach is assumed to be horizontal as well. A breach with the horizontal bottom is also built in CFX. The characteristic size of the soil is another important parameter in the simulation. As shown in Fig. 5, the maximum particle size is around 0.165 m. As suggested by Kang et al. (2017), d_{50} should be used in the simulation. The angle of repose of the material in the dam is close to 45°. According to the correlation between the aggregate angle of friction and the interparticle friction angle proposed by Caquot (1934), the particle contact friction coefficient used in the simulation is equal to 0.64. The parameters in the erosion model calculation are summarized in Table 1.

Rate of erosion
Figure 11 a shows that the drag force at the interface between water and soil increases from the beginning of the simulation to the maximum value of 40.27 N at $t = 80$ s. After that, the drag force starts to decrease until the end of the simulation. Figure 11 b and c show the α_o used in the calculation at different times and the calculated rate of erosion, respectively. Since the height of the first layer in the breach is obtained from field observation, the drag force calculated at the end of 10 s can be used to calculate the rate of erosion between 10 and 20 s. The same characteristic particle size (0.036 m) is used for each layer since the dam material is considered to be homogeneous.

The mean value of α_o in the PDF plays an important role in the erosion calculation. Li and Komar (1986) found that there is a correlation between the pivoting angle (ϕ_p) and α_o, which can be expressed as $\phi_p = (\pi / 2 - \alpha_o)$. Although this correlation is for the natural alluvial material, it at least gives a criterion to determine the mean value of α_o. The mean particle diameter in the simulation is equal to 0.036 m, and the corresponding mean value of α_o, according to the correlation proposed by Li and Komar (1986), is approximately 57°. However, since the dam was built with light compaction, a smaller value should be used. The normal stress increases downward along the depth of the dam, and the corresponding density of the material increases as well. Therefore, it is considered that the value of α_o decreased along the channel depth, as shown in Fig. 11 b.

The rate of erosion is a function of drag force (α_o) and characteristic particle size. For the same particle size, the drag force and the value of α_o together dominate the rate of erosion. The drag force increases with time at the initial 40 s; however, the mean value of α_o decreases with time, resulting in a change of the rate of erosion. Based on the calculation from the progressive scouring model, the maximum rate of erosion is equal to 0.0266 m/s which occurs at a depth between 0.7 and 1.0 m from the initial crest of the dam.

Model setup and flow states
Based on the calculated drag force in the CFX, the rate of erosion can be calculated according to Eqs. (10)–(12). The thickness of a layer is then calculated by multiplying the rate of erosion with a predetermined time period of 5-s interval

Table 1 Parameters used in the calculation of erosion rates

Parameters	Values
Characteristic particle size, d_{50} (m)	0.036
Slope angle, θ (°)	0
Standard deviation of α_0 (°)	0.1
Particle density, ρ_b (kg/m³)	2600
Particle contact friction coefficient	0.64
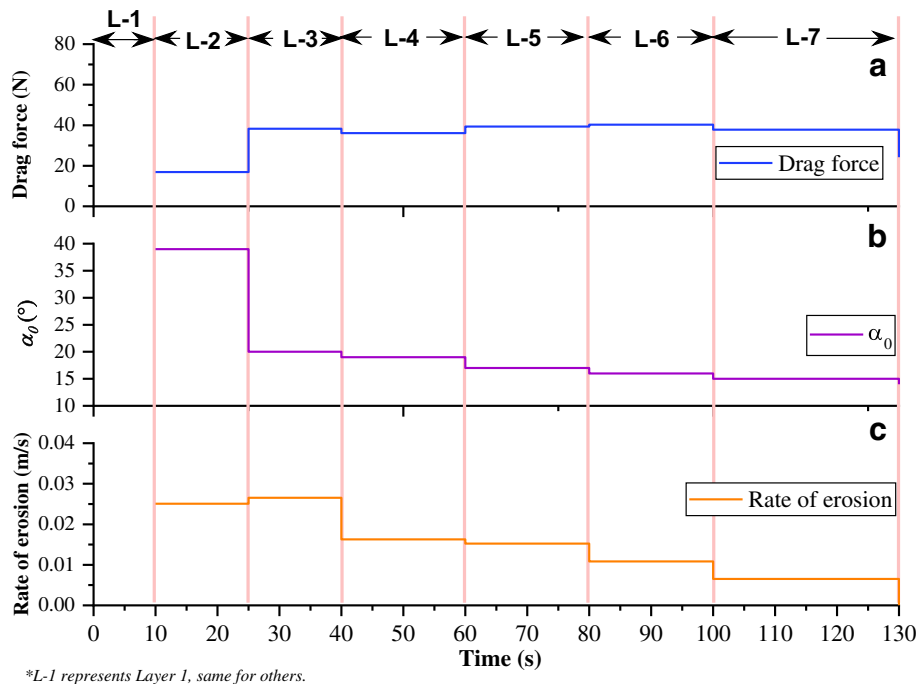
Fig. 11 Erosion model setup and calculation results. **a** Shear stress at the different times. **b** Variation of breach slope angle. **c** Calculated rate of erosion

through a trial and error process (see Table 2). The height of erosion of each layer can be determined through two approaches: changing time duration and changing thickness of erosion. When the time duration is a constant, such as 10 s, the thickness of the eroded layer is very thin at the end of the simulation. However, when a constant thickness is used, the time of erosion is very short at the beginning. To avoid numerical instability for short time durations and to optimize computing time for long durations, both the thickness of the eroded layer and time duration of each eroded layer varied, not in the same time step, during the simulation.

The breaching process is simulated by deleting the layer at a specified time. This calculation is repeated until the end of the breaching process. The breaching process completes in 130 s, and the entire simulation is terminated at 250 s. In the simulation, the breach is divided into seven layers (see Fig. 12). The rates of erosion of each layer range from 0.032 to 0.006 m/s, and a finite volume model composed of multiple erodible layers of elements to simulate the breaching process is built (Fig. 13), which has 793,638 nodes and 3,844,288 elements.

Figure 14 shows the top water surface at different times. The blue region in the figure represents air, and the red represents water. The region showing different water volume fractions is due to the discretization of the domain using finite size elements and the graphical interpolation of air and water in one element. Figure 14 shows more diagrams of the flow conditions at the beginning in a shorter time interval than at the end since more rapid changes in flow condition occur at the beginning of the flow. The flow height of water in the breach at the side close to the reservoir is obviously higher than that at the downstream side. However, when the velocity is high, the height at the outlet of the breach is larger than that in the middle part of the breach.

Analysis of results

Figure 15 compares the observed and calculated surface velocities of water at different times. The surface velocities were measured in the experiment by dropping buoys on the water surface, and the flow conditions were recorded using video cameras at different times. The buoys that gave the best complete flow path were selected to calculate the water surface velocity. In the calculation, the time for a buoy flowing over a short distance at around the middle section of the breach is used. Based on the flowing distance, the velocities in the middle of the breach are calculated, which agree well with field observations (Fig. 15). The root-mean-square error (RMSE) of the calculated velocity in CFX and that of the observed velocity in the initial 50 s are equal to 0.37 m/s. The difference in the calculation is around 16%.

Figure 16 shows the discharge rates calculated using CFX and that based on field observations. Due to the procedure in modeling erosion in the breach using a finite thickness of elements, the discharge rate increases dramatically after a layer is removed, followed by a gradual decrease. The peak discharge rate in the simulation is 10.5 m³/s at $t = 84$ s. Since water is continuously supplied from upstream, the discharge rate finally reaches to a constant value that is very close to the inflow rate.

The discharge rate in the field is also back-calculated according to the changes in the water level on the upstream side. The discharge rate increases to 11.1 m³/s at $t = 70$ s. It starts to decrease except for a sudden increase at approximate $t = 130$ s, which is probably caused by the sudden increase of the cross-sectional area of the breach. The RMSE between the calculated discharge in CFX and the measured discharge in the field is 1.13 m³/s, and the average difference is approximately 6.1%.

After the completion of the breaching of the dam, flow discharge continues since there is a constant inflow of water from the

Table 2 Thickness of each layer in the CFX model of the dam breach

Layers	Starting time (s)	Ending time (s)	Duration (s)	Layer thickness (m)
1	0	10	10	0.329
2	10	25	15	0.369
3	25	40	15	0.324
4	40	60	20	0.365
5	60	80	20	0.294
6	80	100	20	0.229
7	100	250	150	0.248

upstream of the dam in the model and the field. The average inflow rate in the field is approximately 0.5 m³/s.

Discussion of results

The storage capacity of the dam is equal to 1005 m³. The total volume of water inflow during the dam breach process and the volume of water remaining on the upstream side after the dam breach are approximately 125 m³ and 40 m³, respectively, resulting in the total volume of water discharged from the reservoir of about 1090 m³. The discharge rate in the field is back-calculated according to the changes in the water level on the upstream side and the relationship between water level and reservoir volume. The calculated total volume of the water based on the water level in the reservoir can be obtained by integrating the area under the curve in Fig. 16 (area under the light blue line). The total volume from Fig. 16 is calculated to be 1079 m³, showing a discrepancy of approximately 1%. The total volume of water discharged in the CFX model is 1062 m³, showing a difference of 2.5%. In theory, the total volume of water discharged should be the same in all three methods of calculation. The discrepancies possibly come from the following sources: The first possible source of error comes from

the resolution of the DEM, which is used in the calculation of the relationship between water level and the storage capacity of the reservoir. The resolution of the DEM is 0.1 m × 0.1 m, which could result in a difference of about 14 m³ in the total storage capacity. The second possible source of error comes from the relationship used to calculate the discharge rate based on the change in water level. Since the correlation coefficient (R value) of the regression analysis between water level and the reservoir volume is 0.9996, the difference should not be large. The thickness of the layers in the breach in the erosional model is determined based on the calculated discharge rate and water surface on the upstream side. The empirical equations (Eqs. (1) and (2)) are used. Therefore, this may contribute to the error in the water volume calculation.

In the field experiment, the calculated maximum discharge rate and volume of water behind the dam are approximately 11 m³/s and 1005 m³, respectively. The correlation between the maximum discharge and the volume of water behind the dam based on historical dam failure cases is plotted in Fig. 17 a. The regression line shows that the maximum discharge can be correlated with the volume of water behind the dam using a power function, which has a variance of $R^2 = 0.79$ in regression analysis based on the
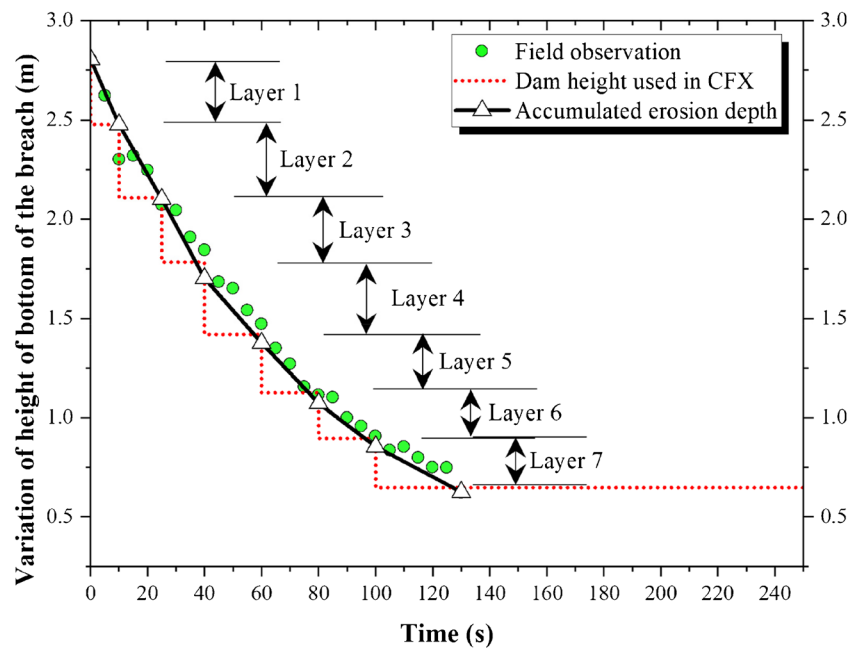
Fig. 12 Comparison of calculated dam height in CFX simulation and field observation
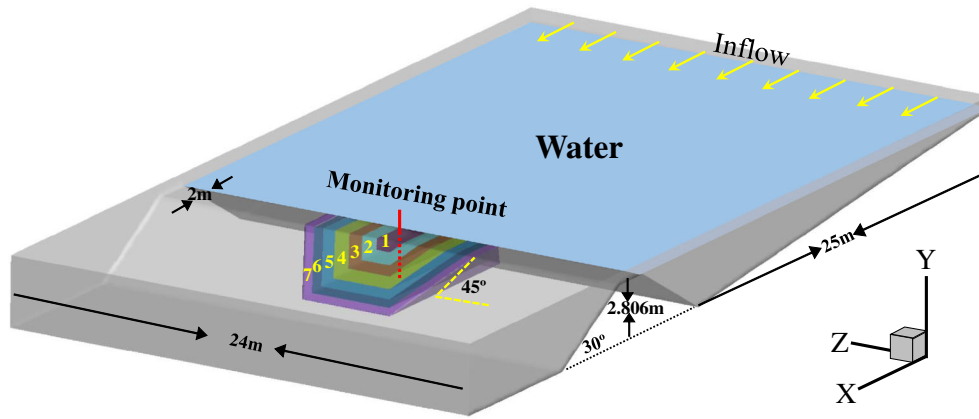
Fig. 13 CFX model of dam and reservoir

collected cases. According to this correlation, the calculated maximum discharge of this field experiment is 8.35 m³/s, when the volume of water is 1005 m³. The discrepancy between the estimated discharge from the correlation above and the calculated discharge based on water level is 24%. The maximum discharges of several laboratory and field experiments are also correlated with the volume of water behind the dam with a variance of $R^2 = 0.97$ based on the summarized experiments (Fig. 17b). The correlation obtained from the field cases shows comparatively large

differences for the maximum discharges of most of the experiments. However, the discrepancies are still within a reasonable range.

In the field, the change in the water surface level and the width at the top of the breach were recorded using a camera. The water level at the upstream face of the dam (h_{up}) and the centerline of the breach can be determined from image analysis of the dam with the help of the gridline on the downstream face. The camera only recorded the first 50 s after the initial dam failure. This is referred
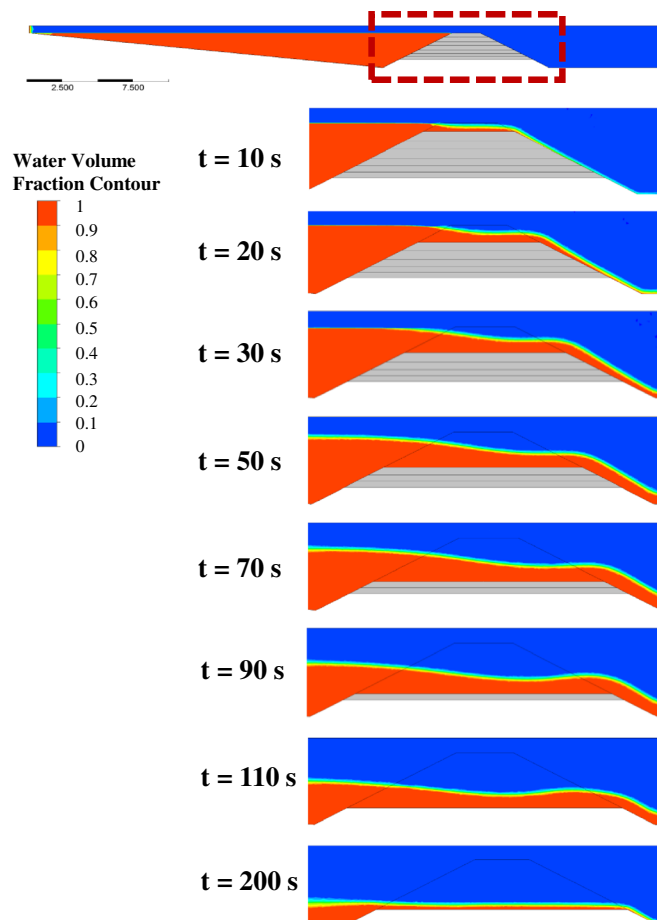

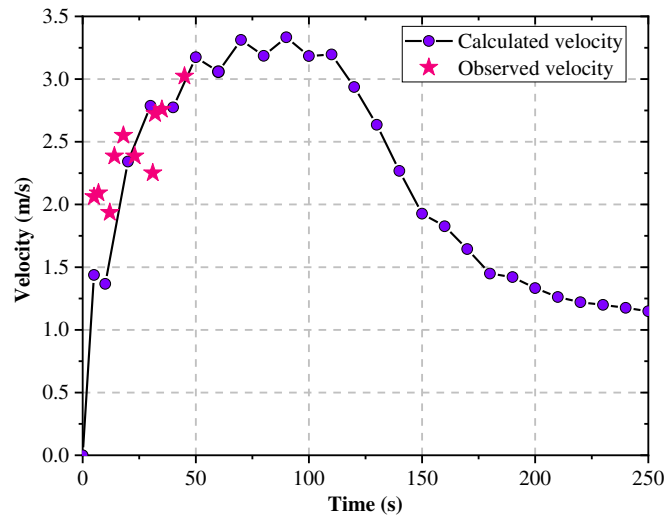**Fig. 14** Water surface at the different times of erosion

Fig. 15 Comparison of the calculated and measured surface velocities of water at the center of the dam

as "Field observation" in Figure 18. The water surface in the middle of the breach can be calculated based on the discharge rate using Eqs. (1) to (3). This is referred as "Back calculation" in Fig. 18. In the simulation, the water surface levels at the upper surface of the dam and the middle of the breach can be obtained. This is referred as "CFX" in Fig. 18. Figure 18 a shows the comparison of water level (h_{up}) based on field observation and CFX which agrees reasonably well with field observations.

Figure 18 b compares the results of the water surface in the middle of the breach ($h_c + h_d$). The results show that there are some discrepancies among the three methods of calculations. The maximum difference between the back-calculated water surface level and the observed water level is approximately 0.2 m. The maximum difference between the observed water level and that calculated using CFX is around 0.1 m. Since the thickness of the layers in the breach and the CFX model is based on field observation, the discrepancy between the water surface levels is not large. This means that the calculation of the height of the bottom of the breach is reasonable. However, in the back-

calculation of the water surface in the middle of the breach, it is assumed that the bottom of the breach is horizontal at all times, which is different from field observation. The erosional model considers changes in the slope of the breach. Therefore, the discrepancy between $h_c + h_d$ obtained in CFX and field observation is smaller than the difference between that obtained in field observation and back-calculation. The results from Fig. 18 a and b show that the consideration of the slope of the bottom of the breach may explain the accuracy in the different methods of calculations.

The width of the top of the breach (B_T) is another indicator that may show the accuracy of the calculation. Figure 18 c shows B_T obtained from the field observation, back-calculation, and CFX simulation. The final width (B_T) is also shown in the figure, which is obtained at the completion of the experiment. The width (B_T) from field observation, in general, is larger than that from back-calculation. The width (B_T) used in the CFX model is calculated using the erosion model. In the calculation, the changes in the slope angle of the bottom of the breach with time are considered.
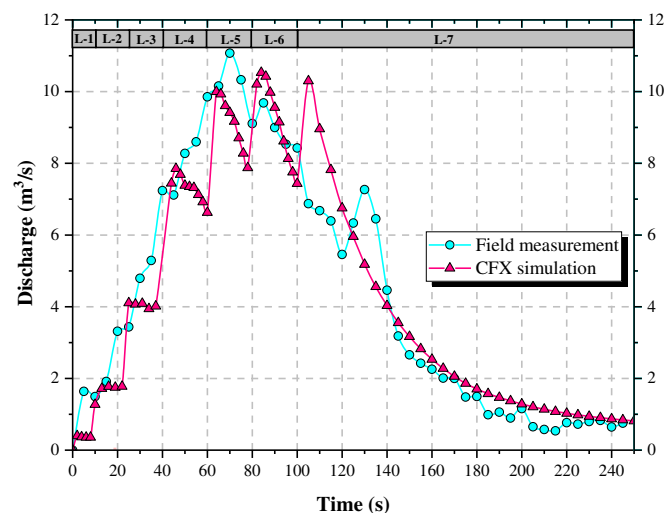

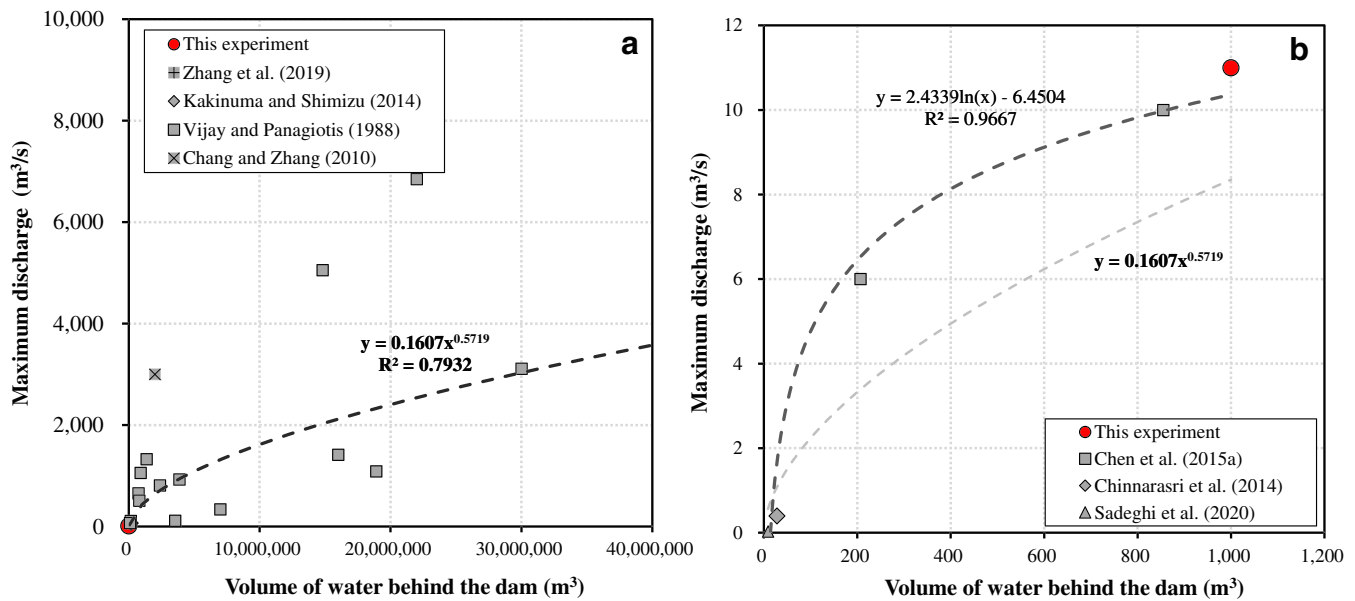**Fig. 16** Measured and calculated discharges at different simulation times

Fig. 17 Correlation between the maximum discharge and volume of water behind the dam before dam failure. **a** Statistical data of field cases and this experiment. **b** Statistical data of laboratory and field experiments

Therefore, the width in the CFX simulation is close to field observation. All calculated final widths (B_T) are smaller than the observed width.

The difference between field observation and that calculated in CFX is also shown in terms of RMSE. The RMSE of the calculated and observed h_{up}, $h_c + h_d$, and B_T values is 0.026 m, 0.095 m, and 0.44 m, respectively. The average differences between the calculated and observed h_{up}, $h_c + h_d$, and B_T values are 1%, 4%, and 13%, respectively. The errors in the simulations using CFX are overall acceptable.

In the calculation of the rate of erosion, both rolling and sliding motions are considered. However, for most erosional models in the literature, mainly including static and dynamic entrainment models (Medina et al. 2008), only sliding motion is considered. For the material in the breach with a buoyancy density of 10 kN/m³ on the channel bed will result in a shear resistance of more than 360 Pa for an internal frictional angle of 45°. However, the calculated maximum shear stress from CFX at the bottom of the breach is only approximately equal to 72.8 Pa, assuming no seepage due to short period of time. This means that the shear resistance is much larger than the applied shear stress, resulting in no calculated erosion if static and dynamic entrainment models are used (see Table 3). The reason for small shear stress is that the shear component is only one part of the drag force in the erosion, which is less than 10% according to the calculation in this simulation. This suggests the erosion models based on the shear failure mechanism underestimate the rate of erosion. Therefore, a particle-scale progressive erosion model with a drag force adopted can overcome this limitation. In conclusion, rolling motion is the dominant mechanism in the erosion process of the breach. This also agrees with the results from triaxial tests of the granular material, showing particle rolling is the major microscopic deformation mechanism (Oda et al. 1982).

Moreover, the calculated surface velocities are also compared with available measured surface velocities in the field in the initial

50 s, as shown in Fig. 15. The overall good agreement suggests that the combined CFX and erosional model is able to simulate the flow and failure process of this dam breach experiment.

Conclusions

A dam breach experiment was carried out using a compacted earth dam constructed in a flow channel in Taiwan. The dam failed by overtopping with water, and failure developed gradually in the lateral and vertical directions. The failure process was simulated using a numerical model.

The variations of the dam height and elevation of the flow channel are calculated based on the digital elevation model of the study area. Assumptions are made to calculate the variation of the height of the bottom of the breach with time at the location of the breach using equations for water flow. The results show that after approximately 130 s, the erosion of the dam reached its maximum depth. The main erosion process took 3–4 min. The maximum discharge agrees well with the correlation between the maximum discharge and the volume of water behind the dam, which are summarized from field cases and other experiments. This demonstrates that the field experiment, in general, has an analogous breaching characteristic as the field cases and other experiments.

An erosional model considering both rolling and sliding motions is incorporated into CFX to calculate the rate of erosion of the breach to simulate the dam breach experiment. The average rate of erosion of the bottom of the breach is approximately 0.017 m/s. The calculation results, such as water level, water surface velocities, and the width of the breach, are compared with field observations with reasonably good agreement. This shows that the erosion model incorporated into CFX is able to capture the main characteristics of the dam failure process. This is a unique full-scale experiment for the evaluation of numerical and analytical models. The results also indirectly show the assumption regarding the erosion process is reasonable, in which the erosion
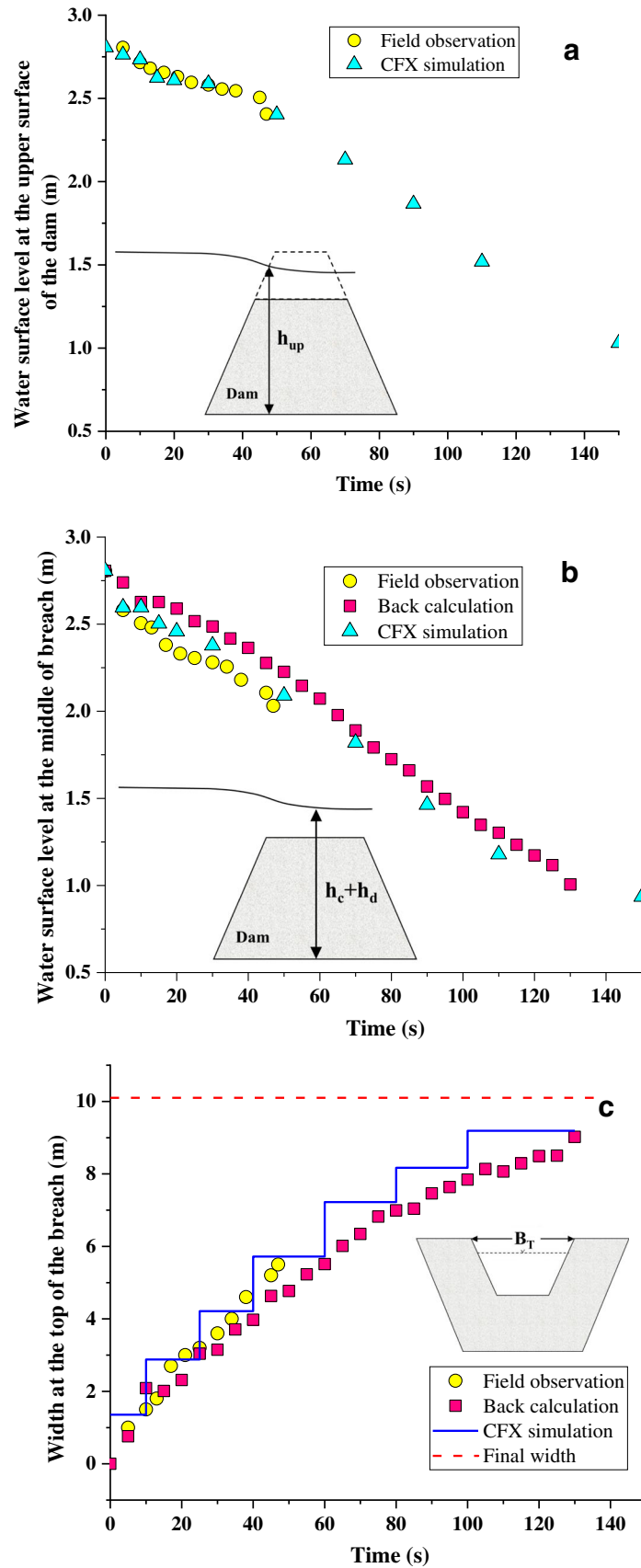
Fig. 18 Comparison of the field observations, back-calculation, and numerical simulations of the **a** water surface level at the upper dam surface, **b** water surface level at the middle of the breach, and **c** the width at the top of the breach

Table 3 Calculated results of the rate of erosion based on the static, dynamic, and progressive scouring entrainment models

Parameters	Entrainment models			Back-calculation based on the water level
	Static	Dynamic	Progressive scouring	
Bulk density (kN/m^3)	20	20	≈ 20	–
Internal friction angle (°)	45	45	45	–
Maximum shear stress (Pa)	72.8	72.8	72.8	–
Shear resistance (Pa)	360	360	–	–
Average rate of erosion (m/s)	0	0	0.017	0.0157

in the breach develops downward and transversely at the same time before reaching the bottom of the dam.

References

Ahmad Z, Azamathulla HM (2012) Quasi-theoretical end-depth–discharge relationship for trapezoidal channels. J Hydrol 456–457:151–155

Alcrudo F, Mulet J (2007) Description of the Tous Dam break case study (Spain). J Hydraul Res 45(sup1):45–57

Azimi AH, Rajaratnam N, Zhu DZ (2013) Discharge characteristics of weirs of finite crest length with upstream and downstream ramps. J Irrig Drain Eng 139(1):75–83

Biscarini C, Di Francesco S, Manciola P (2010) CFD modelling approach for dam break flow studies. Hydrol Earth Syst Sci 14(4):705–718

Blevins RD (1984) Applied fluid dynamics handbook. Van Nostrand Reinhold Co., New York, p 568

Bouchut F, Ionescu IR, Mangeney A (2016) An analytic approach for the evolution of the static-flowing interface in viscoplastic granular flows. Commun Math Sci 14(8):2101–2126

Caquot A (1934) Equilibre des massifs à frottement interne. Gauthier-Villars, Paris (in French)

CFX (2009) ANSYS CFX solver theory guide. ANSYS, Canonsburg

Chang DS, Zhang LM (2010) Simulation of the erosion process of landslide dams due to overtopping considering variations in soil erodibility along depth. Nat Hazards Earth Syst Sci 10(4):933–946

Chen XQ, Cui P, Li Y, Zhao WY (2011) Emergency response to the Tangjiashan landslide-dammed lake resulting from the 2008 Wenchuan earthquake, China. Landslides 8(1):91–98

Chen SC, Feng ZY, Wang C, Hsu TY (2015a) A large-scale test on overtopping failure of two artificial dams in Taiwan. In: Engineering geology for society and territory, 2nd edn. Springer, Cham, pp 1177–1181

Chen Z, Ma L, Yu S, Chen S, Zhou X, Sun P, Li X (2015b) Back analysis of the draining process of the Tangjiashan Barrier Lake. J Hydraul Eng 141(4):05014011

Cheng NS, Law AWK, Lim SY (2003) Probability distribution of bed particle instability. Adv Water Resour 26(4):427–433

Cui P, Dang C, Zhuang JQ, You Y, Chen XQ, Scott KM (2012) Landslide-dammed lake at Tangjiashan, Sichuan Province, China (triggered by the Wenchuan earthquake, May 12, 2008): risk assessment, mitigation strategy, and lessons learned. Environ Earth Sci 65(4):1055–1065

De Blasio FV, Breien H, Elverhoi A (2011) Modelling a cohesive-frictional debris flow: an experimental, theoretical, and field-based study. Earth Surf Process Landf 36(6):753–766

Egashira S, Honda N, Itoh T (2001) Experimental study on the entrainment of bed material into debris flow. Phys Chem Earth, Part C: Solar, Terrestrial & Planetary Science 26(9):645–650

Elkholy M, LaRocque LA, Chaudhry MH, Imran J (2016) Experimental investigations of partial-breach dam-break flows. J Hydraul Eng 142(11):04016042

European Commission (2018) Lao People's Democratic Republic flash flood due to dam collapsing. European Commission Joint Research Centre, Brussels

Fan X, Xu Q, van Westen CJ, Huang R, Tang R (2017) Characteristics and classification of landslide dams associated with the 2008 Wenchuan earthquake. Geoenvironmental Disasters 4(1):12

Gregoretti C, Maltauro A, Lanzoni S (2010) Laboratory experiments on the failure of coarse homogeneous sediment natural dams on a sloping bed. J Hydraul Eng 136(11):868–879

Haun S, Olsen NRB, Feurich R (2011) Numerical modeling of flow over trapezoidal broad-crested weir. Eng Appl Comp Fluid 5(3):397–405

Iverson RM, Ouyang C (2015) Entrainment of bed material by earth-surface mass flows: review and reformulation of depth-integrated theory. Rev Geophys 53(1):27–58

Kakinuma T, Shimizu Y (2014) Large-scale experiment and numerical modeling of a riverine levee breach. J Hydraul Eng 140(9):04014039

Kang C, Chan D (2017) Modelling of entrainment in debris flow analysis for dry granular material. Int J of Geomechanics (ASCE) 17(10):1–20. https://doi.org/10.1061/(ASCE)GM.1943-5622.0000981

Kang C, Chan D (2018a) Numerical simulation of 2D granular flow entrainment using DEM. Granul Matter 20:13. https://doi.org/10.1007/s10035-017-0782-x

Kang C, Chan D (2018b) A progressive entrainment runout model for debris flow analysis and its application. Geomorphology 323:25–40

Kang C, Chan D, Su FH, Cui P (2017) Runout and entrainment analysis of an extremely large rock avalanche—a case study of Yigong, Tibet, China. Landslides 14(1):123–139

Kelbaliyev GI (2011) Drag coefficients of variously shaped solid particles, drops, and bubbles. Theor Found Chem Eng 45(3):248–266

Langford MT, Zhu DZ, Leake A (2016) Upstream hydraulics of a run-of-the river hydropower facility for fish entrainment risk assessment. J Hydraul Eng 142(4):05015006. https://doi.org/10.1061/(ASCE)HY.1943-7900.0001101

Lauber G, Hager WH (1998) Experiments to dambreak wave: horizontal channel. J Hydraul Res 36(3):291–307

Lee SC, Mehta AJ (1994) Cohesive sediment erosion. Dredging research program. Coastal and Oceanographic Engineering Department, Gainesville

Li ZL, Komar PD (1986) Laboratory measurements of pivoting angles for applications to selective entrainment of gravel in a current. Sedimentology 33(3):413–423

Macchione F (2008) Model for predicting floods due to earthen dam breaching. I: formulation and evaluation. J Hydraul Eng-Asce 134(12):1688–1696

Medina V, Bateman A, Hurlimann M (2008) A 2D finite volume model for debris flow and its application to events occurred in the eastern Pyrenees. Int J of Sediment Res 23(4):348–360

Miller S, Chaudhry MH (1989) Dam-break flows in curved channel. J Hydraul Eng-Asce 115(11):1465–1478

Morgenstern, N. R., Vick, S. G., and Z.D., V. 2015. Independent expert engineering investigation and review. Victoria, Canada

Ng CWW, Choi CE, Law RPH (2013) Longitudinal spreading of granular flow in trapezoidal channels. Geomorphology 194:84–93

Oda M, Konishi J, Nemat-Nasser S (1982) Experimental micromechanical evaluation of strength of granular materials: effects of particle rolling. Mech Mater 1(4):269–283

Shi ZM, Guan SG, Peng M, Zhang LM, Zhu Y, Cai QP (2015) Cascading breaching of the Tangjiashan landslide dam and two smaller downstream landslide dams. Eng Geol 193:445–458

Shodja HM, Nezami EG (2003) A micromechanical study of rolling and sliding contacts in assemblies of oval granules. Int J Numer Anal Methods Geomech 27(5):403–424

Shrestha PL, Orlob GT (1996) Multiphase distribution of cohesive sediments and heavy metals in estuarine systems. J Environ Eng-Asce 122(8):730–740

Singh Vijay P, Scarlatos Panagiotis D (1988) Analysis of gradual earth-dam failure. J Hydraul Eng 114(1):21–42

Wu FC, Chou YJ (2003) Rolling and lifting probabilities for sediment entrainment. J Hydraul Eng 129(2):110–119

Yang X, Liu M, Peng S, Huang C (2016) Numerical modeling of dam-break flow impacting on flexible structures using an improved SPH–EBG method. Coast Eng 108:56–64

Zhang JY, Li Y, Xuan GX, Wang XG, Li J (2009) Overtopping breaching of cohesive homogeneous earth dam with different cohesive strength. Sci China Ser E 52(10):3024–3029

Zhang L, Xiao T, He J, Chen C (2019) Erosion-based analysis of breaching of Baige landslide dams on the Jinsha River, China, in 2018. Landslides 16(10):1965–1979

C. Kang (✉) · **D. Chan**
Department of Civil and Environmental Engineering,
University of Alberta,
Edmonton, Canada
Email: ckang3@ualberta.ca

D. Chan
e-mail: dave.chan@ualberta.ca

S. C. Chen · S. Tfwala
Department of Soil and Water Conservation, Innovation and Development Centre of Sustainable Agriculture (IDCSA),
National Chung Hsing University,
Taichung City, Taiwan

S. C. Chen
e-mail: scchen@nchu.edu.tw

S. Tfwala
e-mail: samkelet@gmail.com

D. Chan
College of Civil Engineering and Architecture,
China Three Gorges University,
Yichang, Hubei, China